Journal of The Electrochemical Society, **157** (4) D248-D255 (2010)
0013-4651/2010/157(4)/D248/8/$28.00 © The Electrochemical Society

Electrodeposition of Cu + PdO and (Cu–Pd) + PdO Composites

Enrico Verlato,[a] Sandro Cattarin,[a,*] Nicola Comisso,[a] Rosalba Gerbasi,[b,*] Paolo Guerriero,[b] Marco Musiani,[a,*,z] and Lourdes Vázquez-Gómez[a]

[a]Istituto per l'Energetica e le Interfasi, and [b]Istituto di Chimica Inorganica e delle Superfici, Consiglio Nazionale delle Ricerche, 35127 Padova, Italy

The codeposition of PdO particles with a Cu matrix has been investigated with the aim of extending the composite deposition procedure to the preparation of materials potentially capable of catalyzing the low temperature combustion of methane. Cu + PdO composites with a low dispersed phase content were obtained from either basic pyrophosphate or acid sulfate baths. Codeposition of PdO particles with a Cu–Pd alloy matrix was effectively achieved by electrolyzing suspensions of PdO in solutions containing both Cu^{2+} and Pd^{2+} ions, with large $[Cu^{2+}]/[Pd^{2+}]$ ratios. (Cu–Pd) + PdO deposits with 20–25 Pd atom % were obtained in which only 1–2 atom % of Pd were alloyed in the matrix. These (Cu–Pd) + PdO composites were mechanically stable and highly porous throughout their thickness (their pore volume being ca. 60% of the total volume). Their true surface area was some thousands of times higher than their geometric area.
 [DOI: 10.1149/1.3310021]

Manuscript submitted November 12, 2009; revised manuscript received January 13, 2010. Published March 11, 2010. This was Paper 2728 presented at the Vienna, Austria, Meeting of the Society, October 4–9, 2009.

The low temperature complete oxidation of methane and low hydrocarbons to CO_2 is a process of great fundamental and applied interest[1,2] because the catalytic oxidation process, when employed in power generation, has unique advantages over the conventional thermal combustion process in terms of environmental friendliness. Indeed, it is characterized by very low emissions of residual unreacted methane, which is a much more potent greenhouse gas than CO_2, and is an intrinsically ultralow NO_x process because nitrogen oxide production is negligible at the typical catalytic combustion temperatures (e.g., $\leq$600°C). Many catalytic systems have been investigated with the aim of optimizing their activity and robustness. Most of them consist of composite materials in which particles of the active component are supported on a matrix that may have some direct catalytic activity itself.

Our group has been interested, for over a decade, in the electrodeposition of composite materials for electrocatalysis and has produced, using this approach, both anodes for oxygen evolution reaction (OER)[3] and cathodes for hydrogen evolution reaction (HER).[4] The former electrodes consisted of oxide-matrix composites, deposited at the anode by electrolyzing suspensions of OER catalysts in electrolytes containing either Pb^{2+} or Tl^{+} ions, which were converted to PbO_2 [5,6] and Tl_2O_3,[7,8] respectively. The latter were metal-matrix composites of a very large surface area, produced according to a variant of the pioneering work of Iwakura et al.,[9,10] who extended the composite deposition procedures from the traditional field of surface coatings with enhanced hardness, wear resistance, and self-lubricating properties[11-17] to the production of thin-film materials with a much wider variety of functions.[18]

Our group has recently become interested in exploring the potential of composite electrodeposition in the preparation of materials able to catalyze the low temperature oxidation of methane. There are some affinities between the catalysis of gas-phase reactions and that of electrolytic processes. In both cases, (*i*) having catalysts with an extended surface area is very important because these reactions are heterogeneous and (*ii*) noble metals are among the most active catalytic materials, but because of their high cost, there is a need to limit their amount to a minimum. There are also significant differences; e.g., thermal stability is important for combustion catalysts and much less for electrocatalysts, whereas high electronic conductivity is essential for electrocatalyst matrices and irrelevant for combustion catalysts.

In our exploratory work, the choice of matrix and dispersed phase catalytic materials had to take into account the requirements of the electrodeposition process (i.e., the matrix had to be an electronic conductor that could be easily and effectively deposited) and those of the catalytic combustion (i.e., all materials had to be stable at relatively high temperatures). On the basis of the information in the literature,[1,2] PdO was selected as the dispersed phase. Nickel and copper were considered as possible matrix materials because (*i*) reliable methods for their electrodeposition are available,[19] (*ii*) their melting points (1485 and 1083°C, respectively) are sufficiently high, and (*iii*) their oxides possess themselves some catalytic activity toward methane oxidation[1,2,20,21] and were used as supports for Pd-based catalysts.[22]

Experimental

Chemicals and materials.— $PdO{\cdot}H_2O$ (99.9% purity) was purchased from Alfa Aesar and was used as received. The typical size of most PdO particles, estimated by scanning electron microscopy (SEM), was in the range of 100–300 nm.

The cell used in the voltammetric and electrodeposition experiments consisted of a main central cylindrical compartment, hosting the working electrode (generally rotating at 2000 rpm), connected through glass frits to two lateral compartments, which hosted two Pt wire counter electrodes (overall area 2 cm^2) in the deposition experiments, or a Pt wire counter electrode and a saturated calomel electrode (SCE) in voltammetric experiments; the interelectrode gap was ca. 3.5 cm. All compartments contained the same electrolyte (8 cm^3 in each compartment), but the PdO powders were suspended only in the central one; stirring of the suspensions was provided by a magnetic bar rotating at ca. 1000 rpm. Combining electrode rotation and vigorous stirring of the suspensions was shown to be effective in producing deposits with a homogeneous composition along the disk radius.[5] Unless differently specified, the electrolyte was in contact with the atmosphere, and its temperature was maintained at 25°C with a thermostat.

Cu and Ni disk electrodes [0.2 or 0.3 cm^2 geometric area, with a poly(tetrafluoroethylene) sheath of 1.0 cm diameter], polished with emery paper 1000, rinsed with water, and dried in air, were used as working electrodes. To avoid errors in the determination of the Cu/Pd ratio, which might be caused by sampling the underlying electrode material, alloy and composite samples submitted to the energy-dispersive X-ray (EDX) analyses were always deposited on Ni. The electrochemical equipment consisted of an EG&G potentiostat/galvanostat model 273A, used in voltammetric and electrodeposition experiments, and of an Autolab PGSTAT 100, used in

* Electrochemical Society Active Member.
z E-mail: m.musiani@ieni.cnr.it

electrochemical impedance spectroscopy (EIS) experiments. The SEM analyses were performed with an FEI Quanta 200 FEG ESEM instrument, equipped with a field-emission gun, operating in a high vacuum condition at an accelerating voltage variable from 5 to 30 keV, depending on the observation needs. The EDX analyses were obtained by using an EDAX Genesis EDX spectrometer at an accelerating voltage of 25 keV. The X-ray diffraction (XRD) patterns were obtained by using a Philips X-PERT PW3710 diffractometer with a Bragg–Brentano geometry, employing a Cu Kα source (40 kV, 30 mA).

Procedures.— The electrolytes used in the experiments aimed at depositing Cu–PdO composites were obtained by suspending PdO particles in either of the two Cu electrodeposition baths: (*i*) an acid sulfate bath containing 0.88 M $CuSO_4$ and 0.55 M H_2SO_4 and (*ii*) a mildly basic pyrophosphate bath containing 0.83 M $Na_4P_2O_7$ and 0.17 M $Cu_2P_2O_7$ (pH 8.4). The former is the most common medium for Cu deposition;[19] the latter is a diluted version of another medium recommended by Graham's electroplating handbook.[19] The acid sulfate bath, with the addition of variable concentrations of $PdSO_4$, was used in the deposition of Cu–Pd alloys and, with further addition of PdO, in the deposition of (Cu–Pd) + PdO composites. The voltammetric curves were not corrected for the ohmic drop, which was significant due to the cell geometry and possibly to some contact resistance in the rotating disk electrode (RDE) assembly.

Electrolyses were carried out under galvanostatic control, most often at -50 to -100 mA cm^{-2}. The typical deposition charge was 100 C cm^{-2}, which, in the deposition of pure Cu, would correspond to a deposit thickness of ca. 37 μm if the current efficiency were 100%. The true current efficiency of the deposition processes was estimated from the deposition charge and from the increase in the mass of the electrodes.

The composition of the deposits containing Cu and Pd (formed onto Ni RDEs) was obtained by EDX analyses. Areas of at least 200×200 μm were sampled in these analyses; because the sampling depth was estimated to be a few micrometers, the analyzed deposit volume was ca. 10^7 times the typical particle volume. Therefore, it could be assumed to contain a large number of PdO particles and to be representative of the whole layers. The composition of the deposits, either Cu–Pd alloys or PdO-containing composites, is expressed throughout this paper in terms of Pd atomic percent

$$\text{Pd atom \%} = 100\frac{N_{Pd}}{N_{Pd} + N_{Cu}} \quad [1]$$

where N_{Pd} and N_{Cu} represent atomic concentrations. Other elements, e.g., oxygen, were neglected in the calculations.

Some voltammetric experiments aimed at assessing the feasibility of the codeposition of the PdO particles with a Ni matrix were carried out using a conventional Watt's bath: 1.126 M $NiSO_4 \cdot 6H_2O$, 0.185 M $NiCl_2 \cdot 6H_2O$, and 0.485 M boric acid, pH 4, kept at 55°C.[19]

The EIS and voltammetric tests aimed at characterizing the composite roughness and composition were carried out in a two-compartment cell, with working and counter electrodes in the main compartment and an SCE, used as reference, connected through a Luggin capillary. In the EIS experiments, the working electrode was polarized at its open-circuit potential; the frequency range of 100 mHz to 100 kHz was covered with eight points per decade and the amplitude of the modulated potential was 10 mV rms. Some voltammetric experiments were carried out with Pd sheet electrodes (0.4 cm^2 area) after their electrochemical or thermal (2 h at 450°C) oxidation.

Results and Discussion

Voltammetric study of PdO codeposition with Ni or Cu.— A preliminary study aimed at assessing whether PdO particles could be deposited with either a Ni or a Cu matrix was carried out by cyclic voltammetry. The results are shown in Fig. 1 and 2, respectively.

Curve A in Fig. 1 shows that the only reduction process observed by sweeping the potential of a Cu RDE from the open-circuit value

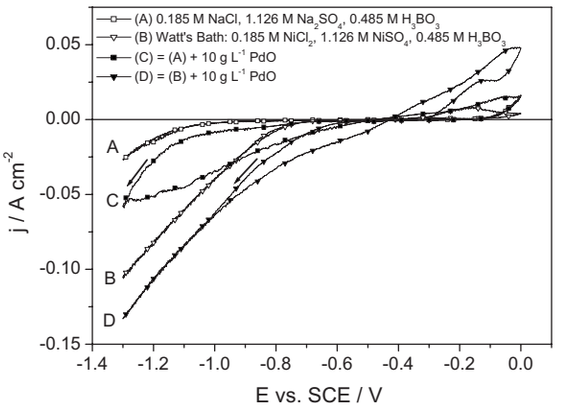

Figure 1. CVs recorded with a Cu RDE (2000 rpm) in (curve A) 0.185 M NaCl, 1.126 M Na_2SO_4, and 0.485 M H_3BO_3; (curve B) 0.185 M $NiCl_2 \cdot 6H_2O$, 1.126 M $NiSO_4 \cdot 6H_2O$, and 0.485 M H_3BO_3; (curve C) 0.185 M NaCl, 1.126 M Na_2SO_4, 0.485 M H_3BO_3, and 10 g L^{-1} PdO; (curve D) 0.185 M $NiCl_2 \cdot 6H_2O$, 1.126 M $NiSO_4 \cdot 6H_2O$, 0.485 M H_3BO_3, and 10 g L^{-1} PdO. All solutions had pH 4 and were kept at 55°C; sweep rate of 100 mV s^{-1}.

toward more negative potentials in a mildly acid NaCl, Na_2SO_4, and H_3BO_3 solution was HER, which became evident at $E < -1.0$ V. Curve B in the same figure shows that when Na salts were replaced by the corresponding Ni salts, so as to obtain a classical Watt's bath,[19] a current due to the Ni deposition flowed at $E < -0.7$ V. Curve C, relevant to a sodium salt solution in which PdO particles were suspended, shows a negative current at $E < -0.65$ V, thus suggesting that PdO was electroactive because no other species could be reduced. The current measured in the reverse sweep (toward positive E) was more negative than that measured in the forward sweep and was still negative at -0.50 V. Such a behavior is typical of the nucleation of a new solid phase on the electrode surface. After prolonged polarization of the electrode in the potential range between -0.7 and -1.2 V, very thin, very poorly adherent, gray deposits were seen. Curve D shows that the onset of a reduction current was shifted to a less negative potential when PdO particles were suspended in the Watt's bath; at all $E < -0.60$ V, the reduction current was higher in the presence than in the absence of PdO. In the potential range between -1.0 and -0.45 V, the current was more negative during the reverse than during the forward

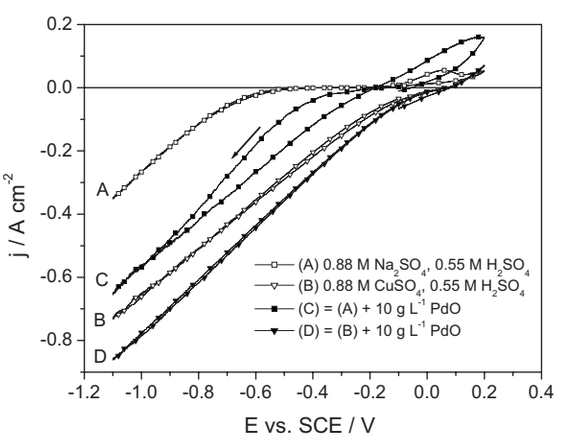

Figure 2. CVs recorded with a Ni RDE (2000 rpm) in (curve A) 0.88 M Na_2SO_4 and 0.55 M H_2SO_4; (curve B) 0.88 M $CuSO_4$ and 0.55 M H_2SO_4; (curve C) 0.88 M Na_2SO_4, 0.55 M H_2SO_4, and 10 g L^{-1} PdO; and (curve D) 0.88 M $CuSO_4$, 0.55 M H_2SO_4, and 10 g L^{-1} PdO; sweep rate of 100 mV s^{-1}.

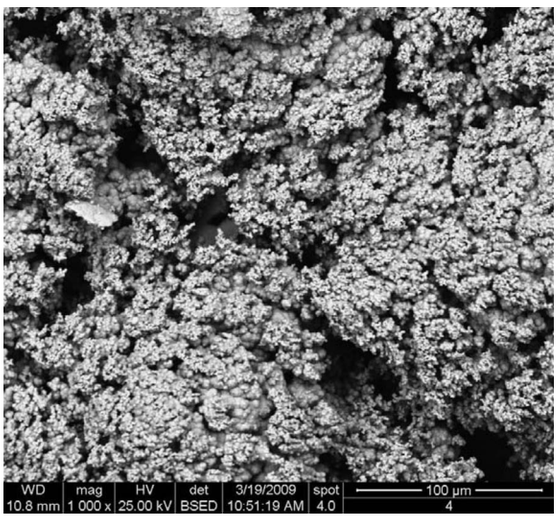

Figure 3. SEM image of a Cu + PdO deposit obtained by cathodic deposition from 0.83 M $Na_4P_2O_7$, 0.17 M $Cu_2P_2O_7$, and PdO 10 g L^{-1} (pH 8.4) with a −100 mA cm^{-2} deposition current density.

sweep. Also in this case, the deposits formed on the electrode were very thin and adhered to the electrode very poorly.

A similar set of experiments, relevant to Cu deposition onto a Ni RDE, is shown in Fig. 2. Curve A shows that HER took place at $E < -0.45$ V in a Na_2SO_4 and H_2SO_4 solution. Copper deposition from a $CuSO_4$ and H_2SO_4 solution occurred at a much more positive potential ($E < 0.07$ V), as shown by curve B. Curve C shows that the PdO particles were electroactive when suspended in the Na_2SO_4 and H_2SO_4 solution; the fact that the current was more negative during the reverse than during the forward sweep suggests that a deposit was formed. However, the electroactivity of PdO was observed only at potentials more negative than those necessary to Cu deposition (comparing curves B and C), at variance with the behavior observed with Ni (Fig. 1). When the PdO particles were suspended in $CuSO_4$ and H_2SO_4 solution, no significant potential shift was observed in the onset of Cu deposition; the only significant effect of the PdO particles was enhancing the reduction current (curve D).

The comparison of Fig. 1 and 2 suggests that the electroactivity of the PdO particles (which may be due both to their reduction when they are brought in contact with the electrode surface and to the catalysis of HER by Pd formed at the PdO surface and deposited on the electrode) prevents the effective deposition of Ni. Instead, Cu may be deposited in a potential range where PdO is inactive, at less negative potentials than Ni, and so Cu and Cu matrix composites can be grown. Indeed, prolonged electrolyses carried out in the $CuSO_4$ and H_2SO_4 solution with suspended PdO particles led to the formation of thick deposits, as described below. The current enhancement due to the PdO particles (comparing curves C and D in Fig. 2) probably originated from different phenomena: simultaneous Cu^{2+} and PdO reduction, enhanced HER, and deposition of rougher deposits, with a larger effective area (see below). Results similar to those in Fig. 2 were obtained with the Cu pyrophosphate deposition bath.

Deposition of Cu + PdO composites from basic copper pyrophosphate solutions.— According to the Pourbaix diagrams, PdO is quite unstable toward dissolution at pH < 1. Therefore, although the most common Cu deposition bath is a sulfate bath with pH ca. 0,[19] to operate with solutions in which PdO was stable, we initially attempted the deposition of Cu + PdO composites using basic copper pyrophosphate solutions. Figure 3 shows an SEM image of a Cu + PdO deposit obtained from 0.83 M $Na_4P_2O_7$, 0.17 M $Cu_2P_2O_7$, and 10 g L^{-1} PdO (pH 8.4) with a −100 mA cm^{-2} current density. Under these and similar conditions, thick and porous deposits were obtained, with a current efficiency close to 100%, but this system had several drawbacks: The Pd content in the deposits was limited to ≤2 atom %, the deposits were rather brittle and their adhesion to the substrate was rather poor. Furthermore, probably due to local pH changes, precipitation of some salt, possibly a basic Cu pyrophosphate, occurred simultaneously to deposit formation. For all these reasons, this route was abandoned.

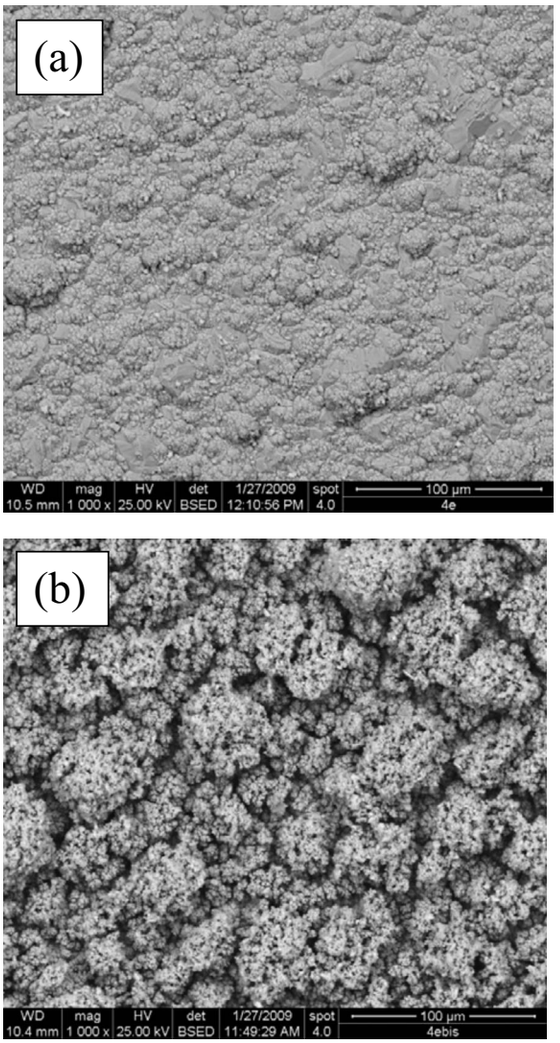

Figure 4. SEM images of deposits obtained by cathodic deposition from 0.88 M $CuSO_4$, 0.55 M H_2SO_4, and 10 g L^{-1} PdO, with a −50 mA cm^{-2} deposition current density. Deposit (a) was obtained from a freshly prepared suspension; deposit (b) was obtained from a suspension stirred during ca. 3 h.

Deposition of Cu + PdO and (Cu–Pd) + PdO composites from acid copper sulfate solutions.— Several deposition experiments were carried out in succession by imposing a −50 mA cm^{-2} deposition current density to Ni cathodes rotating at 2000 rpm in the same 0.88 M $CuSO_4$, 0.55 M H_2SO_4, and 10 g L^{-1} PdO suspension. The deposition charge was 100 C cm^{-2}, and so the duration of each electrolysis was 2000 s. Deposits were formed in all electrolyses with a current efficiency close to 100%, i.e., with negligible gas evolution side reactions. A comparison of the SEM images of deposits obtained from (a) a freshly prepared suspension and from (b) a suspension stirred during ca. 3 h is shown in Fig. 4. A marked

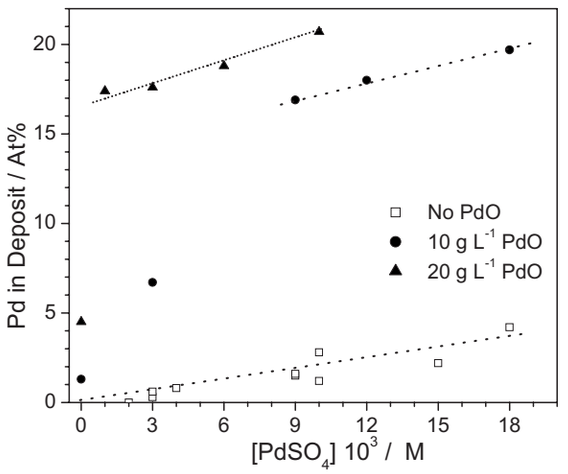

Figure 5. Dependence of the composition of Cu–Pd and (Cu–Pd) + PdO deposits on the concentration of $PdSO_4$ added to 0.88 M $CuSO_4$ and 0.55 M H_2SO_4 solutions containing no (□), 10 g L^{-1} (●), or 20 g L^{-1} (▲) PdO in suspension. Deposition current density and deposition charge were −50 mA cm^{-2} and 100 C cm^{-2}, respectively. The lines are just guides for the eyes.

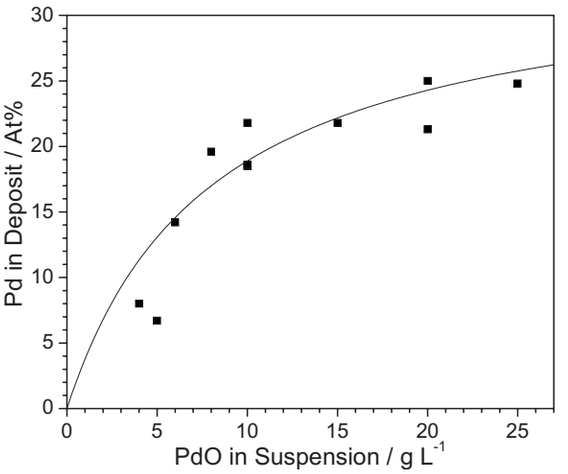

Figure 6. Dependence of the composition of (Cu–Pd) + PdO deposits on the concentration of PdO suspended in 0.88 M $CuSO_4$, 0.55 M H_2SO_4, and 0.006 M $PdSO_4$ solutions. Deposition current density and deposition charge were −50 mA cm^{-2} and 100 C cm^{-2}, respectively. The continuous curve, calculated according to $Pd_{deposit} = 34 \times [1.25PdO_{suspension}/(1 + 1.25PdO_{suspension})]$, is a guide for the eyes.

increase in the deposit roughness from (a) to (b) is evident. EDX analyses of the samples shown in Fig. 4 showed that the Pd contents were 1.9 and 8.7 atom %, respectively.

This evolution in the composition of the deposits can be interpreted by taking into account that the equilibrium condition[23] for the reaction

$$PdO + 2H^+ = Pd^{2+} + H_2O \quad [2]$$

is

$$\log[Pd^{2+}] = -2.35 - 2pH \quad [3]$$

and therefore PdO should dissolve in a strongly acidic solution, to reach an equilibrium concentration of 4.5×10^{-3} M in a pH 0 solution. Simultaneous reduction of Cu^{2+} and Pd^{2+} might then lead to the formation of a Cu–Pd alloy,[24-26] with a consequent increase in the Pd content of the deposit. According to Simonet et al.,[27] Pd spontaneously deposits on Cu from acid sulfate solutions of Pd^{2+}, and this might be another possible route for the entry of Pd in the deposit.

The dissolution kinetics of PdO (10 g L^{-1}) in a 0.88 M Na_2SO_4 and 0.55 M H_2SO_4 solution was monitored by recording the UV/visible spectra of solution samples after various interaction times. During the first 6 h, the Pd^{2+} concentration increased, essentially linearly, by 1.6×10^{-3} M/h, to yield a Pd^{2+} concentration in excess of that given by Eq. 3, which neglects the effect of sulfate anions.

Cu–Pd alloys were deposited from 0.88 M $CuSO_4$ and 0.55 M H_2SO_4 solutions containing variable concentrations of $PdSO_4$, at a −50 mA cm^{-2} current density, and were submitted to the EDX analysis. Figure 5 (□) shows that for Pd^{2+} concentrations in the range of 0–18×10^{-3} M, the Pd content in the alloy varied roughly linearly and never exceeded 5 atom %. The Pd content in the alloys increased quite sharply as the Pd^{2+} concentration was further increased (data not shown in Fig. 5). The dependence of the composition of deposits obtained from 0.88 M $CuSO_4$ and 0.55 M H_2SO_4 solutions containing 10 or 20 g L^{-1} PdO on Pd^{2+} concentration was then investigated. Data are shown in Fig. 5 [(●) and (▲), respectively]. In these experiments, a freshly prepared suspension was used in each electrolysis, and thus, PdO dissolution might cause an increase in the Pd^{2+} concentration by 9×10^{-4} M at most. Figure 5 shows that the Pd content in these samples was much higher than that in the alloys obtained with the same $[Cu^{2+}]/[Pd^{2+}]$ ratio without suspended PdO. Therefore, it can be concluded that composites were formed in which the PdO particles were dispersed in a Cu–Pd alloy matrix; henceforth, these materials will be denoted as (Cu–Pd) + PdO. The difference in the Pd content between (Cu–Pd) + PdO composites and Cu–Pd alloys increased as $[Pd^{2+}]$ increased to become essentially independent of it. The Pd content in the (Cu–Pd) + PdO composites obtained with $[Pd^{2+}]$ in the range of 3–18×10^{-3} M was much higher than the sum of the Pd content in the alloys (obtained without suspended PdO) and the Pd content in the Cu + PdO composites (obtained in the absence of Pd^{2+} in solution), thus suggesting a catalytic effect. In principle, two alternative explanations may be proposed for the phenomena shown in Fig. 5: (*i*) The presence of Pd^{2+} in the deposition bath enhanced the deposition rate of PdO, which was codeposited more effectively with a Cu–Pd alloy than with pure Cu, or (*ii*) the presence of PdO in the suspension enhanced the atomic fraction of Pd in the Cu–Pd alloys formed at the cathode. This issue is discussed below on the basis of the XRD data.

The data in Fig. 5 allows us to interpret the dependence of the deposit composition on the number of successive electrolyses performed with the same suspension (see above discussion of Fig. 4): As the duration of the interaction between the PdO particles and the acid solution increased, the Pd^{2+} concentration in the solution built up, the matrix material deposited at the cathode changed from essentially pure Cu to Cu–Pd alloys, and composites with a high content of either alloyed Pd(0) or PdO were formed.

Figure 5 also shows that the overall Pd content was higher for samples prepared with the higher amount of PdO in suspension [(▲) vs (●)]. This issue was further investigated by varying the amount of PdO suspended in 0.88 M $CuSO_4$, 0.55 M H_2SO_4, and 0.006 M $PdSO_4$ solutions (again, freshly prepared suspensions were used in each experiment). The results are shown in Fig. 6, where the experimental data are roughly interpolated by a curve that phenomenologically reproduces the behavior predicted by the Guglielmi model.[28] This curve shows that in spite of some data scattering (somewhat larger than the error expected in the EDX analyses), the composition of (Cu–Pd) + PdO composites depends on the PdO concentration in a way commonly observed for many composite deposition systems: When the dispersed phase concentration in the suspension is progressively increased, its concentration in the deposit increases markedly at first and then more weakly up to a limiting value.

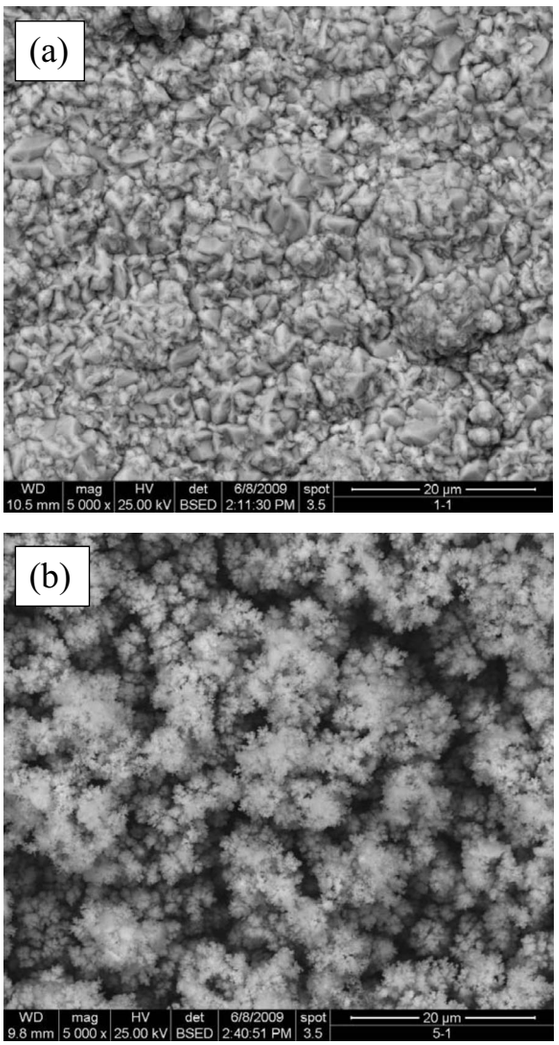

Figure 7. SEM images of deposits obtained from 0.88 M $CuSO_4$, 0.55 M H_2SO_4, and 0.003 M $PdSO_4$ solutions in which (a) no PdO or (b) 10 g L^{-1} PdO were suspended. In both cases, deposition current density and deposition charge were −50 mA cm^{-2} and 100 C cm^{-2}, respectively.

Characterization of (Cu–Pd) + PdO deposits.— Figure 7 shows the SEM images of a Cu–Pd alloy obtained from a (a) 0.88 M $CuSO_4$, 0.55 M H_2SO_4, and 0.003 M $PdSO_4$ solution and of a (b) (Cu–Pd) + PdO composite obtained from an identical solution in which 10 g L^{-1} PdO was suspended. The EDX analyses showed that these samples contained 0.6 and 6.7 Pd atom %, respectively. Clearly, besides increasing the Pd content, codeposition of PdO particles induced a marked increase in the deposit roughness. Such a behavior is commonly observed when particles of sufficiently high electronic conductivity are used as dispersed phases in composite deposition[29] and has been exploited in the preparation of electrocatalysts with a large effective area.[3,5-8,18,30]

To obtain a quantitative estimate of the effective area of the alloy and composite deposits, their impedance was measured in an inert electrolyte (0.5 M Na_2SO_4), so as to determine the double-layer capacity of the electrodes, which, in the first approximation, may be assumed to be proportional to the true area, irrespective of the sample composition. Figure 8a shows the plots of the imaginary part of the impedance vs frequency, in logarithmic–logarithmic coordinates, for a Cu electrode polished with Al_2O_3 and for Cu, Cu–Pd, and (Cu–Pd) + PdO electrodeposits; the impedance of each electrode was measured at its open-circuit potential (−0.025, −0.04, +0.015, and −0.02 V, respectively). None of the electrodes had an ideal capacitive behavior, which agrees with Härtinger and Doblhofer,[31] who reported that deviations in the impedance of Cu electrodes immersed in neutral media from an ideally capacitive behavior were caused by OH^- electrosorption. However, a fairly wide frequency range (delimited in Fig. 8a by a couple of vertical dotted lines) in which the slope of the curves approached −1 could be identified in each plot. For Cu and Cu–Pd alloy electrodes, this range was found at medium-high frequency, whereas for the (Cu–Pd) + PdO composite a capacitive behavior was best approached at much lower frequencies (between 0.1 and 10 Hz). The latter behavior is typical of porous electrodes, the capacity of which is equal to that of a flat electrode of the same area as the developed pore surface, and can be measured only at frequencies low enough that the ac signal penetration depth is as large as the pore depth.[32] At higher frequencies (e.g., 50–2000 Hz), the plot relevant to the (Cu–Pd) + PdO composite shows a linear branch with a slope close to −1/4; in a Nyquist plot of the impedance of the (Cu–Pd) + PdO composite (Fig. 8b) the high frequency linear portion forms with the real axis an angle close to 22.5°, much smaller than 45°, the value expected for cylindrical pores.[33] Similar results were previously reported by Gourbeyre et al.,[34] who ascribed them to the presence of branched pores.

The surface roughness of each electrodeposit (defined as the ratio between its true surface area and its geometric area) was obtained by dividing its capacity by the capacity of the polished Cu electrode (which is equivalent to assuming the latter to be ideally flat). Because the impedance response of the electrodes was never ideally capacitive, the linear portions of the impedance plots (Fig. 8a) were analyzed, assuming a series resistance-constant phase element (R-CPE) combination as a model, with the CPE impedance given by

$$Z_{\mathrm{CPE}} = \frac{1}{Q(j\omega)^{\alpha}} \qquad [4]$$

The parameters Q and α were evaluated by the graphical method proposed by Orazem et al.,[35] and the effective double-layer capacity was computed according to the formula proposed by Brug et al.[36] for blocking electrodes

$$C_{\mathrm{eff}} = Q^{1/\alpha} R^{(1-\alpha)/\alpha} \qquad [5]$$

The surface roughness of the Cu electrodeposit was only marginally higher than that of polished Cu. The Cu–Pd alloy had a markedly higher surface roughness (5.8). The surface roughness of the composite was as high as 7300, ca. 3 orders of magnitude higher than that of the alloy. In spite of the coarse approximations (i.e., assuming the double-layer capacity of the unit electrode surface to be independent of the electrode composition and the polished Cu electrode to be ideally flat), the results in Fig. 8 prove the major effect of codeposition of PdO particles on the true surface area of the deposits.

Figure 9 shows a fracture section of a (Cu–Pd) + PdO deposit grown to a thickness of ca. 200 μm. Both magnifications show that the deposit is highly porous throughout its whole depth and that pores with sizes variable from a few micrometers down to 100 nm or less are present. The thickness of the sample shown in Fig. 9 was quite constant along its radius, and thus its total volume could be easily calculated with fairly good precision. From the deposition charge, the volume of deposited Cu was estimated (neglecting other components of the deposits). By comparing these two volumes, it was estimated that the pore volume was ca. 60% of the total volume. Some Cu–Pd alloys with up to 25 Pd atom % were deposited from Cu^{2+} and Pd^{2+} acid sulfate solutions with appropriate $[Cu^{2+}]/[Pd^{2+}]$ concentration ratios. SEM images and impedance measurements, not reported here, showed that their surface roughness was significantly higher than that of the sample shown in Fig. 7a. Although the Cu–Pd alloys were not investigated in detail, it may be speculated

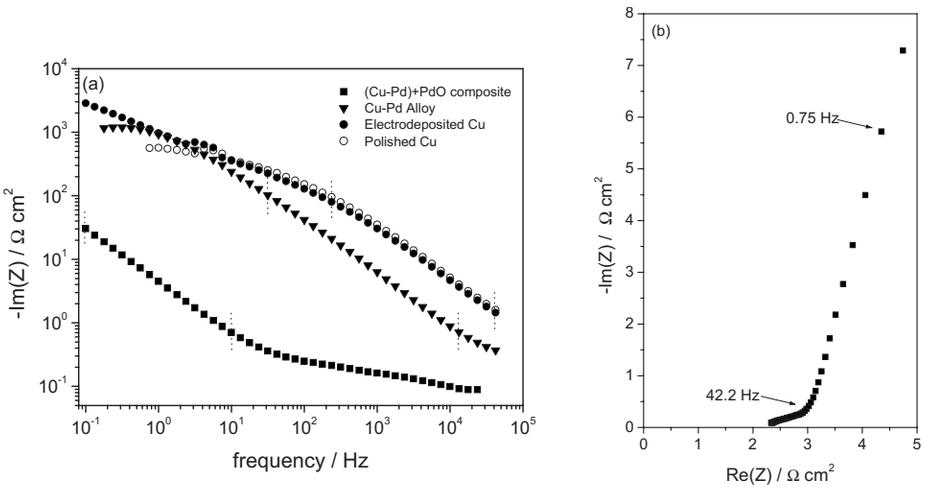

Figure 8. (a) Frequency dependence of the imaginary part of the impedance of Cu [(○) polished; (●) electrodeposited], Cu–Pd (▼), and (Cu–Pd) + PdO (■) electrodes, measured in 0.5 M Na_2SO_4, at the respective open-circuit potentials. (b) Nyquist plot of the impedance of the (Cu–Pd) + PdO electrode.

that they might provide a route to the deposition of porous Pd-containing materials onto substrates of complicated geometry for which composite deposition might be ineffective.

Further work was aimed at establishing the chemical status of the Pd atoms contained in the deposits. The cyclic voltammogram (CV) of a (Cu–Pd) + PdO deposit was recorded in a 0.5 M Na_2SO_4 solution (in which, due to the absence of electroactive species, only redox processes involving the electrode material or the solvent are possible) and compared to those of oxidized Pd electrodes and of a Cu electrodeposit. The results are shown in Fig. 10. The potential of the thermally oxidized Pd electrode was swept at first toward a negative potential (curve A): A reduction peak was observed at −0.54 V, which may be attributed to the PdO reduction,[37] followed at more negative potentials by water reduction (with hydrogen adsorption, absorption, and evolution). In the reverse sweep, peaks at 0.42 and 0.82 V may be ascribed to the reoxidation of hydrogen and Pd. For electrochemically oxidized Pd (curve B), the potential of a polished Pd electrode was swept at first toward positive potentials (up to 1.7 V, not shown in Fig. 10), causing Pd oxidation; a reduction peak was observed at −0.13 V, suggesting that the species produced by electrochemical oxidation, presumably more strongly hydrated, was easier to reduce than the thermal oxide. A weak reduction peak around −0.12 V was observed also for the Cu electrodeposit (curve C); it is ascribed to the reduction of CuO formed by atmospheric oxidation and upon immersion of the electrode in the Na_2SO_4 solution. Finally, the voltammogram of (Cu–Pd) + PdO showed reduction peaks at −0.28 and −0.43 V during the initial sweep toward negative potentials (curve D). These peaks are compatible with the reduction of both CuO and incorporated PdO particles. The Cu and (Cu–Pd) + PdO deposits were obtained with the same deposition charge; the much larger reduction current measured in the latter case was probably a result of the much larger surface area of the composite deposit.

Figure 11 shows the X-ray diffractograms of (A) the as-purchased PdO powder used in the electrodeposition experiments, (B) an electrodeposited Cu_{77}–Pd_{23} alloy, and [(C) and (D)] two electrodeposited (Cu–Pd) + PdO composites. The PdO diffractogram shows very broad and not very intense peaks, located at angles, which agree with the literature,[38] which show that the PdO powders were almost amorphous (the crystal size estimated by the Scherrer formula is in the range of 20–30 Å). The diffractogram of the Cu–Pd alloy shows a set of peaks located at positions intermediate between those of Cu [39] and those of Pd [40] (at variance with Milhano et al.,[26] who reported the Cu–Pd alloys deposited from perchlorate solutions to be amorphous). Both Cu and Pd crystallize in the cubic system, and their lattice parameters are 3.6150 and 3.8902 Å, respectively. The lattice parameter of the Cu–Pd alloy was calculated to be 3.670, which, assuming that the lattice parameter varies linearly with the atomic fraction of the alloy components, corresponds to a $Cu_{80}Pd_{20}$ composition; such a composition agrees well with the EDX analysis of the same sample, considering the precision of the analyses and

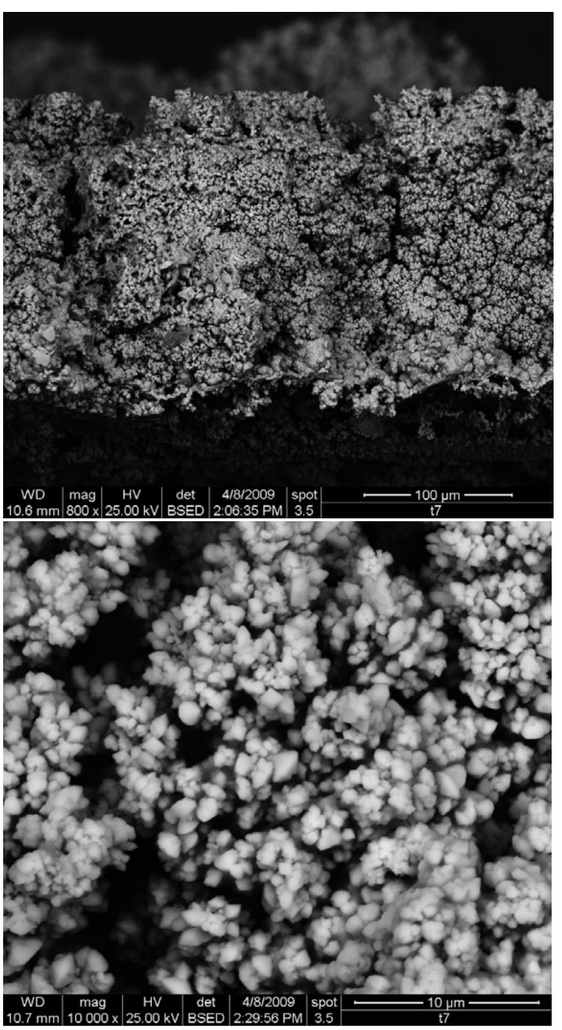

Figure 9. SEM images, at two different magnifications, of a fracture section of a (Cu–Pd) + PdO composite.

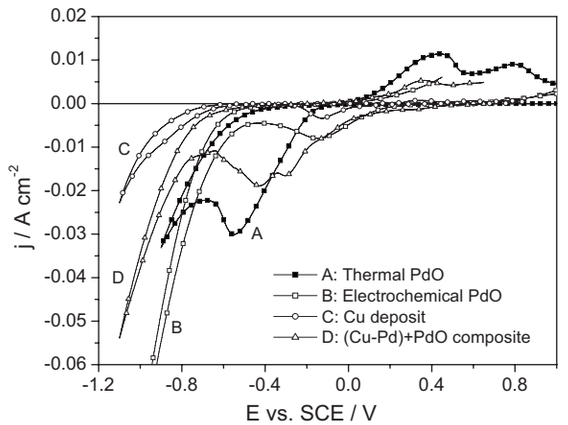

Figure 10. CVs obtained with thermally or electrochemically oxidized Pd, Cu, or (Cu–Pd) + PdO electrodes in 0.5 M Na_2SO_4; sweep rate of 100 mV s^{-1}.

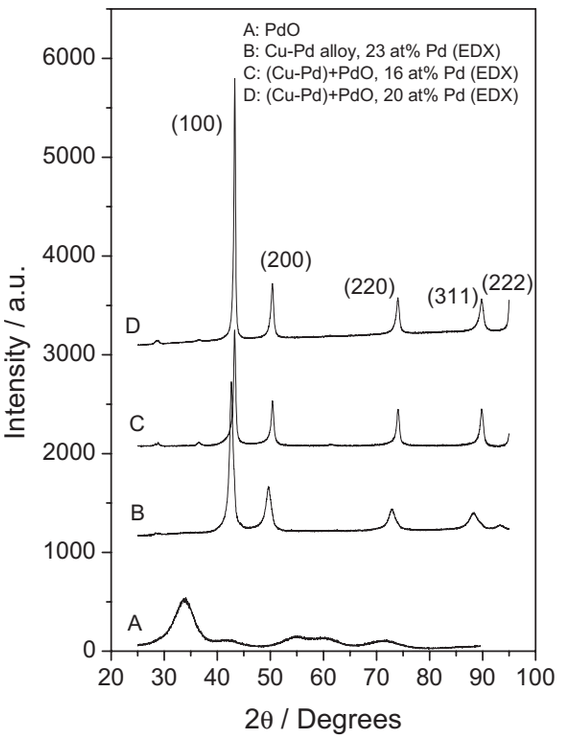

Figure 11. X-ray diffractograms of (A) as-purchased PdO powder, (B) electrodeposited Cu–Pd alloy, and [(C) and (D)] electrodeposited (Cu–Pd) + PdO composites. The overall Pd contents in the electrodeposits, determined by EDX, were (B) 23, (C) 16, and (D) 20 atom %. The diffractograms are shifted along the intensity axis for the sake of clarity.

the possible deviations from Vegard's law. The diffractograms of the (Cu–Pd) + PdO composites, which contained 16 and 20 atom % Pd, respectively (determined by EDX), showed peaks at positions fairly close to those of pure Cu. Calculations of the lattice parameters and, hence, of the composition of the crystalline component of the deposits yielded $Cu_{98.3}Pd_{1.7}$ and $Cu_{97.8}Pd_{2.2}$ for their matrices. Therefore, one can conclude that only a minor fraction of the Pd atoms contained in the (Cu–Pd) + PdO composites were present as alloyed Pd(0) in the matrix, while the large majority was present as embedded PdO, or possibly as Pd generated by PdO reduction. The fact that the reflections typical of PdO (notably the most intense one expected at 33.84°) were absent from the diffractograms [(C) and (D)] is not surprising if the quasi-amorphous nature of PdO is considered.

The XRD data in Fig. 11 allow us to rule out the hypothesis that the Cu–Pd alloys obtained in the presence of suspended PdO are much richer in alloyed Pd than those obtained in its absence. In fact, the Pd content of the matrices is comparable with those of alloys obtained in the absence of suspended particles. Thus, one must conclude that the codeposition of PdO particles becomes much more effective as soon as matrices consisting essentially of Cu contain as little as 1–2 atom % Pd. To the best of our knowledge, this is an uncommon phenomenon in composite electrodeposition, which can be tentatively explained by supposing that the reduction of Pd^{2+} ions adsorbed at the PdO surface greatly facilitates the PdO incorporation in the matrix.[11]

Conclusions

An exploratory study on the possibility of codepositing PdO particles with metal matrices, so as to obtain porous composite materials potentially able to catalyze the low temperature combustion of methane, has led to the following conclusions:

1. Codeposition of PdO with a Ni matrix is precluded because at the fairly negative potentials at which Ni^{2+} is reduced, PdO is electroactive; its cathodic reactions and, most probably, water reduction at Pd centers prevent the effective deposition of a robust Ni matrix able to incorporate Pd.
2. Codeposition of PdO with a Cu matrix is possible, both from basic pyrophosphate and acid sulfate baths.
3. The deposits obtained from basic pyrophosphate baths are brittle, have scanty adherence to the substrates, and have low Pd content (typically <2 atom %). Furthermore, these baths are difficult to handle.
4. PdO is not fully stable in the acid sulfate bath as it undergoes dissolution to give Pd^{2+}. The dissolution process causes a continuous variation in the composition of the deposition baths and therefore in the composition and properties of the materials deposited therefrom.
5. Unexpectedly, the presence of low concentrations of Pd^{2+} (2 orders of magnitude below $[Cu^{2+}]$) strongly favors the codeposition of PdO. (Cu–Pd) + PdO composites with overall Pd content above 20 atom % are thus easily obtained; in these deposits, ca. 1/10 of the Pd atoms are alloyed with Cu in the matrix, the others being present as PdO particles, possibly partly reduced to Pd.

The catalytic properties of the (Cu–Pd) + PdO composites will be tested in a successive stage of this project.

Acknowledgments

The authors acknowledge the financial support of the Italian Ministry for Economic Development (MSE), MSE-CNR Agreement on National Electrical System. The authors are indebted to the FILA INDUSTRIA CHIMICA SPA, San Martino di Lupari, Padova, Italy, owner of the Fei-ESem FEI Quanta 200 FEG instrument for allowing its use for the research work described in this paper.

References

1. T. V. Choudhary, S. Banerjee, and V. R. Choudhary, *Appl. Catal., A*, **234**, 1 (2002).
2. P. Gélin and M. Primet, *Appl. Catal., B*, **39**, 1 (2002).
3. S. Cattarin and M. Musiani, *Electrochim. Acta*, **52**, 2796 (2007).
4. L. Vázquez-Gómez, S. Cattarin, P. Guerriero, and M. Musiani, *Electrochim. Acta*, **52**, 8055 (2007).
5. M. Musiani, F. Furlanetto, and P. Guerriero, *J. Electroanal. Chem.*, **440**, 131 (1997).
6. M. Musiani, F. Furlanetto, and R. Bertoncello, *J. Electroanal. Chem.*, **465**, 160 (1999).
7. M. Musiani and P. Guerriero, *J. Electrochem. Soc.*, **145**, 549 (1998).
8. M. Musiani, F. Furlanetto, and P. Guerriero, *J. Electrochem. Soc.*, **145**, 555 (1998).
9. C. Iwakura, N. Furukawa, and M. Tanaka, *Electrochim. Acta*, **37**, 757 (1992).
10. C. Iwakura, M. Tanaka, S. Nakamatsu, H. Noue, M. Matsuoka, and N. Furukawa,

Electrochim. Acta, **40**, 977 (1995).
11. J. R. Roos, J. P. Celis, J. Fransaer, and C. Buelens, *J. Met.*, **42**, 60 (1990).
12. J. P. Celis, J. R. Roos, C. Buelens, and J. Fransaer, *Trans. Inst. Met. Finish*, **69**, 133 (1991).
13. C. Buelens, J. Fransaer, J. P. Celis, and J. R. Roos, *Bull. Electrochem.*, **8**, 371 (1992).
14. J. Fransaer, J. P. Celis, and J. R. Roos, *Met. Finish.*, **91**, 97 (1993).
15. A. Hovestad and L. J. J. Jansen, *J. Appl. Electrochem.*, **25**, 519 (1995).
16. C. T. J. Low, R. G. A. Wills, and F. C. Walsh, *Surf. Coat. Technol.*, **201**, 371 (2006).
17. A. Hovestad and L. J. J. Jansen, in *Modern Aspects of Electrochemistry*, B. E. Conway, C. G. Vayenas, R. E. White, and M. E. Gamboa-Adelco, Editors, Vol. 38, p. 475, Kluwer, New York (2005).
18. M. Musiani, *Electrochim. Acta*, **45**, 3397 (2000).
19. A. K. Graham, *Electroplating Engineering Handbook*, pp. 231–257, Van Nostrand Reinhold, New York (1971).
20. M. C. Marion, E. Garbowski, and M. Primet, *J. Chem. Soc., Faraday Trans.*, **86**, 3027 (1990).
21. J. G. McCarthy, Y.-F. Chang, V. L. Wong, and M. E. Johansson, *Prepr., Pap. - Am. Chem. Soc., Div. Fuel Chem.*, **42**, 158 (1997).
22. T. Ishihara, H. Shigematsu, Y. Abe, and Y. Takita, *Chem. Lett.*, **3**, 407 (1993).
23. M. Pourbaix, *Atlas d'Equilibres Electrochimiques*, p. 358, Gauthier-Villars & Cie, Paris, France (1963).
24. R. Lacmann, *Electrochim. Acta*, **34**, 1225 (1989).
25. D.-L. Lu, M. Ichihara, and K. Tanaka, *Electrochim. Acta*, **43**, 2325 (1998).
26. C. Milhano and D. Pletcher, *J. Electroanal. Chem.*, **614**, 24 (2008).
27. J. Simonet, P. Poizot, and L. Laffont, *J. Electroanal. Chem.*, **591**, 19 (2006).
28. N. Guglielmi, *J. Electrochem. Soc.*, **119**, 1009 (1972).
29. T. W. Andersen, C. H. Pitt, and L. S. Livingston, *J. Appl. Electrochem.*, **13**, 429 (1983).
30. H. J. Miao and D. L. Piron, *Electrochim. Acta*, **38**, 1079 (1993).
31. S. Härtinger and K. Doblhofer, *J. Electroanal. Chem.*, **380**, 185 (1995).
32. J.-P. Candy, P. Fouilloux, M. Keddam, and H. Takenouti, *Electrochim. Acta*, **26**, 1029 (1981).
33. R. de Levie, in *Advances in Electrochemistry and Electrochemical Engineering*, P. Delahay, Editor, Vol. VI, p. 329, Interscience, New York (1967).
34. Y. Gourbeyre, B. Tribollet, C. Dagbert, and L. Hyspecka, *J. Electrochem. Soc.*, **153**, B162 (2006).
35. M. E. Orazem, N. Pébère, and B. Tribollet, *J. Electrochem. Soc.*, **153**, B129 (2006).
36. G. J. Brug, A. L. G. van den Eeden, M. Sluyters-Rehbach, and J. H. Sluyters, *J. Electroanal. Chem. Interfacial Electrochem.*, **176**, 275 (1984).
37. M. Grdeń, M. Łukaszewski, G. Jerkiewicz, and A. Czerwiński, *Electrochim. Acta*, **53**, 7583 (2008).
38. ICDD card 41-1107 (1989).
39. ICDD card 04-0836 (1953).
40. ICDD card 46-1043 (1993).